An environmentally friendly approach for the synthesis of Au nanoparticles supported mesoporous silica for catalytic applications

ANDRÉS GUZMÁN-CRUZ[1], F. PARAGUAY-DELGADO[2], MOU PAL[1,*]

[1]Instituto de Física
Benemérita Universidad Autónoma de Puebla
Apdo. Postal J-48, Puebla 72570
MEXICO

[2]Departamento de Materiales Nanoestructurados
Centro de Investigación en Materiales Avanzados (CIMAV)
Av. Miguel de Cervantes 120, Complejo Industrial Chihuahua, Chihuahua 31136
MEXICO

Abstract: - Mesoporous silica has received much attention as an attractive support material for metal nanoparticles (NPs) with good dispersion and exceptional stability for various catalytic reactions. However, the lack of synthetic protocols to controlled synthesis of mesoporous silica with high surface area and ideal pore size for supporting metal NPs significantly reduces the catalytic performance and stability of the catalysts. This work reports a facile synthetic route to prepare mesoporous silica-supported Au NPs (Au/SiO_2) for efficient catalytic reduction of 4-nitrophenol. An environmentally friendly synthetic route was exploited to prepare mesoporous silica using deep eutectic solvent (DES) derived from choline chloride/urea as an efficient solvent and template in solvothermal reaction. The mesoporous silica was first functionalized with $–NH_2$ groups, and subsequently, Au NPs with an average size of 10 nm were deposited onto the mesoporous silica matrix. Owing to the strong interaction of supported Au NPs with the mesoporous silica support, the resultant composite exhibited excellent catalytic performance towards the reduction of 4-NP to 4-aminophenol with a rate constant of K_{app}= 3.04 $x10^{-1}$ min^{-1} and exceptionally high stability compared to bare mesoporous silica catalyst. The current green approach to fabricating mesoporous silica and Au/SiO_2 catalysts holds great promise since it is a much cheaper and environmentally friendly method for large-scale fabrication of other supported catalysts for different catalytic reactions.

Key-words: Deep eutectic solvent, green synthesis, mesoporous SiO_2, Au/SiO_2, catalytic reaction, 4-nitrophenol reduction

Received: May 2, 2022. Revised: May 23, 2022. Accepted: May 25, 2022. Published: June 2, 2022.

1 Introduction

With the progress in nanotechnology, gold nanoparticles have attracted considerable interest for their applications in different fields such as catalysts in remediation of water pollution [1], plasmon mediated enhancement in solar cell efficiency [2], biosensors [3], antimicrobial activity [4] and targeted drug delivery for cancer therapy [5]. Compared to other noble metals, Au NPs have several advantages which include biocompatibility, resistance to oxidation, and surface plasmon resonance in visible spectral range [6]. The physical and chemical properties of gold NPs are primarily governed by size, shape and surface properties. Small gold nanoparticles with size below 10 nm often serve as good catalysts due to their high surface area, and lower coordination number of the large fraction of gold surface atoms which make them chemically active [7]. However, due to the high surface energy, the small Au NPs tend to agglomerate into larger particles, which leads to catalyst deactivation. To overcome this shortcoming and reduce the cost of catalysts, various support materials are proposed including TiO_2, SiO_2, CeO_2, Fe_3O_4, Cu_2O and Al_2O_3 [8-13]. SiO_2 is recognized as a good support material for Au NPs because of its high thermal stability, superior mechanical strength, chemically inertness towards Au, easy synthetic route and uniform size [14]. Sol gel is the widely used

method to synthesize SiO_2 nanoparticles because of its several advantages such as low temperature process and easy control of reaction kinetics by changing the composition of the reactives, pH, reaction time, etc. [15]. Other methods such as reverse micro-emulsion, solution combustion synthesis, hydrothermal method, ultrasonic spray pyrolysis are also employed to obtain nanosized SiO_2 [16]. Similar to sol-gel method, hydro/solvothermal method is particularly malleable as the morphological properties can be tailored by varying reaction temperature, time, pH and use of additives. In this process, the reaction is conducted at the temperature higher than the boiling point of the solvent inside a reactor. The autogenous pressure created inside the reactor breaks the existing bonds in the reactives and produces the new chemical bond in the product. Therefore, solvent plays a central role in this method. Recently, deep eutectic solvents (DES) are emerging as promising class of solvents and are explored frequently for the preparation of metal oxides. This type of solvents is eutectic mixture of molecular and ionic compounds acting as hydrogen bond donors (HBDs) and hydrogen bond acceptors (HBAs). Usually, primary amines, carboxylic acids, amides, and alcohols serve as HBDs as they have polar N-H and O-H groups. While, quaternary amine salts such as choline chloride (ChCl) is a popular HBA compound for this purpose. ChCl-urea mixture (reline) is prototype example of this category of solvent which is formed by mixing urea (mp 133 °C) and ChCl (303 °C) at eutectic molar ratio of 2:1 having a freezing point of 12 °C. Like most of the DES, reline exhibits chemical stability, low volatility, nontoxicity and noninflammability. Besides its role as solvent, DES serves as templating agent due to their extensive H- bonding network, which helps to form porous structure in resulting nanoparticles [17]. The combination of solvothermal process with the unusual properties of reline eutectic solvent is expected to produce SiO_2 nanoparticles with advantageous properties.

On the other hand, Au NPs are traditionally deposited on metal oxide surface by coprecipitation and deposition-precipitation process using $HAuCl_4$ as Au-precursor. The size and size distribution of gold NPs are highly dependent on the precursor concentration, the relation of molar ratio between gold precursor and reducing agent and pH of the solution [14].

Supported gold NPs are proven to be efficient in different catalytic reactions such as oxidation of alkanes and alcohols [3], oxidation of CO, oxidative decomposition of volatile organic compounds and hydrogenation of aromatic nitro compounds [7]. 4-Nitrophenol (4-NP) is an important raw material for the manufacturing of dyes, paints, medicines, pigments and fertilizers. Due to its wide application, 4-NP is a common organic pollutant in industrial waste water and its removal is a top priority. Compared to the traditional methods, catalytic hydrogenation of 4-NP is more effective using noble metal catalysts as can be observed in previous literature [18].

In this communication, we report the synthesis of Au/SiO_2 nanocomposites using a combination of solvothermal and borohydride reduction method. The resulting composites were characterized by X-ray diffraction (XRD), Raman scattering, UV-Visible diffuse reflectance spectroscopy (DRS), transmission electron microscopy (TEM), scanning electron microscopy (SEM), energy dispersive X-ray spectroscopy (EDS) and BET measurements. The effect of gold concentration in precursor solution has been studied using Au/SiO_2 composites as catalysts in 4-NP hydrogenation.

2 Experimental

2.1 Materials

Choline chloride ($HOC_2H_4N(CH_3)_3Cl$ ≥98%), urea ($CO(NH_2)_2$) ≥98%), tetraethyl orthosilicate (TEOS, 98%), nitric acid (HNO_3 66.30%), ethanol (CH_3CH_2OH 100%), (3-Aminopropyl)triethoxysilane (APTES ≥98%) and sodium borohydride ($NaBH_4$ ≥98%) were purchased from sigma Aldrich, Mexico. All the chemicals used as received and deionized (DI) water was used for throughout the experimental synthesis.

2.2. Preparation of ChCl/urea based DES (*reline*)

First, ChCl was dried in an oven at 95 °C for 1 h in order to remove the adsorbed water. Thereafter, urea was added into ChCl in a molar ratio of 2:1 and heated at 95°C to obtain a homogeneous and viscous liquid which was used as solvent for the synthesis of SiO_2.

2.3. Synthesis of SiO_2 nanoparticles

SiO_2 NPs were prepared by DES-assisted solvothermal method. In a typical synthesis, an acidic

aqueous solution was prepared by mixing 0.15 mL of nitric acid in 4.7 mL of deionized water and stirred for 10 min. Then, 10.15 mL of TEOS was added to the mixture and stirred for another 20 min at room temperature. Finally, the precursor solution was mixed with 10 mL of DES *reline* and stirred for 30 min to obtain a viscous gel-like solution. The mixture was transferred to Teflon lined stainless steel autoclave and heated at 100 ^{o}C for 24 h inside an air-circulating oven under autogenous pressure. After cooling to room temperature, the solid white product was washed repeatedly with water and ethanol by centrifugation at 9,000 rpm for 15 min and dried at 60 ^{o}C for 6 h.

2.4 Incorporation of Au NPs on SiO_2 support

Au/SiO_2 nanocomposite was prepared by the reduction of Au (III) ions over amine-functionalized SiO_2 surface using APTES as fuctionalizasing agent and sodium borohydride as a reducing agent. In a typical process, 300 mg of prefabricated SiO_2 was dispersed in 100 mL of anhydrous ethanol under magnetic stirring for 1h. Then, 1 mL of concentrated APTES was added to the mixture and allowed to stirred for another 6h at 60°C to obtain amine ($-NH_2$) functionalized SiO_2 surface. After that, the surface functionalized SiO_2 (SiO_2-NH_2) was recovered by centrifugation, washed with ethanol and dried at 60°C for 3h. Subsequently, 100 mg of dry SiO_2-NH_2 powder was dispersed in 100 mL of ethanol and then 5 mL of $HAuCl_4$ solution (1 mM and 2.5 mM) was added to it. The mixture was stirred magnetically for 20 min to disperse the gold ions over functionalized SiO_2 surface. Afterward, 5 mL of $NaBH_4$ solution (1mM) was added to the mixture, and the reaction was left to constant stirring for another 20 min at room temperature. A red color precipitate was formed indicating the reduction of Au^{3+} ions into Au^0. The product was recovered by centrifugation at 15,000 rpm for 15 min and washed several times with ethanol to discard the unreacted Au precursor and borohydride solution. The precipitate was dried at 60 °C for 3h to obtain a reddish pink powder of Au/SiO_2 composite. The Au/SiO_2 samples were labelled as SA1 and SA2 for using 1 mM and 2.5 mM gold precursors, respectively.

2.5. Materials characterization

Powder XRD patterns of SiO_2 and Au/SiO_2 composites were obtained using a Malvern Panalytical-Empyrean X-ray diffractometer with Cu K_α emission (λ = 1.5406 Å) in the 2θ range of 10°-90°. Raman spectroscopy was performed using a Raman microscopy system (Jobin Yvon LabRAM HR800 system) equipped with an Olympus BX41 microscope to focus the laser light. A He-Ne laser (λ_{exc} = 632.8 nm) served as excitation source. The surface morphology of the particles was inspected by JEOL JEM 2200FS transmission electron microscope with an accelerating voltage of 100 kV. SEM and EDS measurements were performed on an HITACHI (Model: SU8230) scanning microscope with 30.0 kV acceleration voltage. The optical properties of the samples were evaluated on a Varian (Agilent) Cary 5000 UV-Vis spectrophotometer with diffuse Reflectance Accessory (DRA-CA-30I). The N_2-absorption/desorption isotherms were obtained utilizing a Belsorp Mini-II sorptometer (BEL, Japan) at 77 K after degassing at 180^{o} C for 15 h.

2.6. Catalytic reduction of 4NP

The catalytic reduction of 4-NP using SiO_2 and Au/SiO_2 catalysts was conducted using $NaBH_4$ as described in the literature [14]. First, 8 mL of 4-NP solution (0.2 mM) was mixed with 16 mL of DI water in a glass vial resulting in a light yellow color solution. After that, 30 mg of $NaBH_4$ was added into it and the color changes to bright yellow. The absorption spectra of 4-NP taken before and after the addition of borohydride indicates a shift of absorption band from 317 nm to 400 nm due to the formation of 4-nitrophenolate ions under basic conditions (Fig. 7a). Then, 4 mg of SiO_2 or Au/SiO_2 nanocomposite was added to the solution. The absorption spectra were recorded at every 2 min by withdrawing an aliquot of 2 mL and separating the catalyst through filtration using a reusable syringe (z268410) fitted with a nitrocellulose membrane filter of 0.22 μm pore size.

3 Results and discussion

3.1 Textural properties of SiO_2 support

Eutectic solvents play an important role as dispersion medium and create interparticle voids among the SiO_2 nanoparticles. It is desirable that the support materials has large surface area to provide more active sites for gold deposition. To analyze the specific surface area, BET N_2 adsorption-desorption measurements have been performed and shown in Figure 1(a). Our SiO_2 NPs exhibit a reverse S-shape isotherm, which is

classified as type IV isotherm corresponding to the mesoporous structure in SiO_2. Notably, the filling of the multilayers takes place at low relative pressure in the range of 0.1 – 0.6 with a steep rise due to the condensation of the mesopores at relative pressure in the range of 0.6 – 0.94 and finally a plateau-shaped region is reached, indicating complete filling of mesopores at relatively high pressure. In this case, the hysteresis loop is Type H1, which refers to a mesoporous material with uniform cylindrical or columnar pore [19]. Fig. 1(b) presents the pore size distribution of SiO_2 sample and revels a dominant pore diameter centered at around of ~ 6 nm. BET specific surface area (SSA) of SiO_2 sample was ~ 347.83 m^2/g, which is much higher than other SiO_2 material reported previously such as commercial SiO_2 (175-225 m^2/g) [20], SiO_2 nanoparticles (180 m^2/g) [21], silica microspheres (21.28 m^2/g) [22] and SiO_2 particles (6.3547 m^2/g) [23], suggesting that the present synthesis route is effective to obtain a mesoporous material.

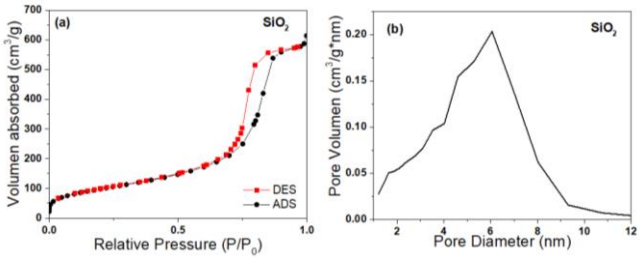

Fig. 1. (a) Nitrogen adsorption and desorption isotherms of the as-synthesized SiO_2 and (b) shows the pore-size distribution of SiO_2 support.

3.2 XRD analysis

Fig. 2 shows the diffraction pattern of bare SiO_2 and Au/SiO_2 nanoparticles obtained with different concentration of gold precursor. For all the samples, a broad diffraction peak centered at 2θ = 22.49º is observed, corresponding to amorphous phase of SiO_2. For Au/SiO_2 nanocomposites, apart from the SiO_2 peak, four well-defined and sharp diffraction peaks are located at 2θ = 38.26°, 44.38, 64.62°, 77.67° and 81.85°, which match well with the peak positions of face-centered cubic (FCC) phase of gold (JCPDS # 04-0784). Furthermore, the intensity of gold diffraction peaks increases with increasing $HAuCl_4$ concentration from 1mM to 2.5 mM, suggesting the formation of larger size and/or highly loaded gold NPs. The crystallite size of Au NPs loaded on SiO_2 is calculed using the well-known Scherrer equation, revealing grain size of 8.67 nm and 11.9 nm for SA1 and SA2, respectively. The obtained results indicate that Au nanoparticles are effectively deposited on SiO_2 support.

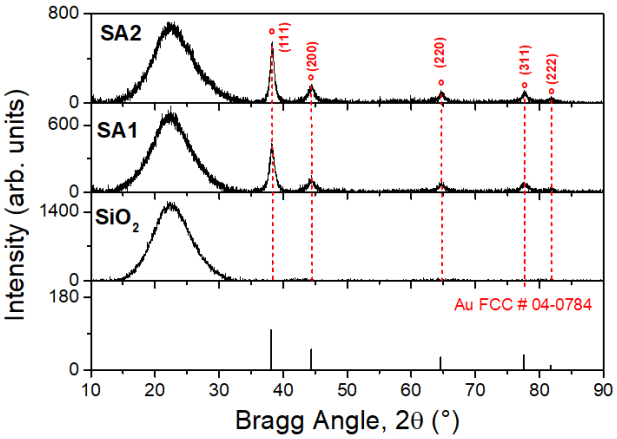

Fig. 2. X-ray diffraction patterns of (a) SiO_2 and Au/SiO_2 obtained with different concentration of Au(III) precursor: (b) 1 mM y (c) 2.5mM.

3.3. TEM measurements

Fig. 3 shows low-resolution TEM images of SiO_2 and Au/SiO_2 nanoparticles. For bare SiO_2, mesoporous nanoparticles can be seen which are interconnected with each other by irregular-shape wormhole type framework. The size distribution histogram (inset of Fig. 3a) reveals an average particle size of ~9.9 nm. For Au/SiO_2 samples, we can observe the formation of dark and semi-spherical gold nanoparticles dispersed on the surface of SiO_2 (grey background). The size of gold NPs is found to be relatively inhomogeneous. The average particle size for SA1 and SA2 are 9 ±3.56 nm and 19 ± 8.85 nm, respectively as shown in the particle size distribution histograms (insets of Fig. 3b and 3c). From TEM images, it is clear that by increasing the concentration of gold precursor, more gold nanoparticles of bigger size are loaded on SiO_2 surface.

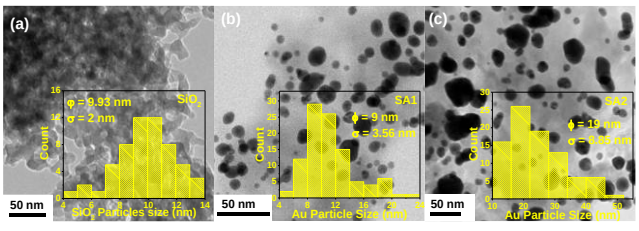

Fig. 3. Typical TEM images of (a) SiO_2 and Au/SiO_2 with different concentration of Au^{3+} (b) 1 mM y (c) 2.5mM. The size distribution histograms of gold NPs

are shown in the insets of Fig. 3a, b & c where φ and σ represents mean size and standard deviation, respectively.

3.3 Scanning electron microscopy (SEM) and energy dispersive X-ray spectroscopy (EDS) measurements

Fig. 4 a-c shows the low and high magnification SEM images of Au/SiO_2 composite (SA2) and corresponding EDS-elemental mapping analysis. From Fig. 4a, b, we can see the spherical Au nanoparticles supported over mesoporous SiO_2. A close inspection of a high magnification SEM image (Fig. 4c) reveals that Au NPs with a particle size of ca. 10 nm are slightly agglomerated, which could be attributed to the nonuniform functionalization of SiO_2 surface by $-NH_2$ groups using APTES. EDS-mapping analysis confirms that Au NPs are incorporated throughout the SiO_2 matrix with fair dispersion along with few aggregates, as displayed in Fig. 4d. Furthermore, EDS- spectrum (Fig. 5) revealed the presence of only Si, O, and Au elements were detected, and no additional peaks associated with DES components were observed, suggesting the purity of the obtained Au/SiO_2 nanocomposite. The estimated Au-content from the EDS quantification analysis was about 3.70 wt% in the Au/SiO_2 nanocomposite sample.

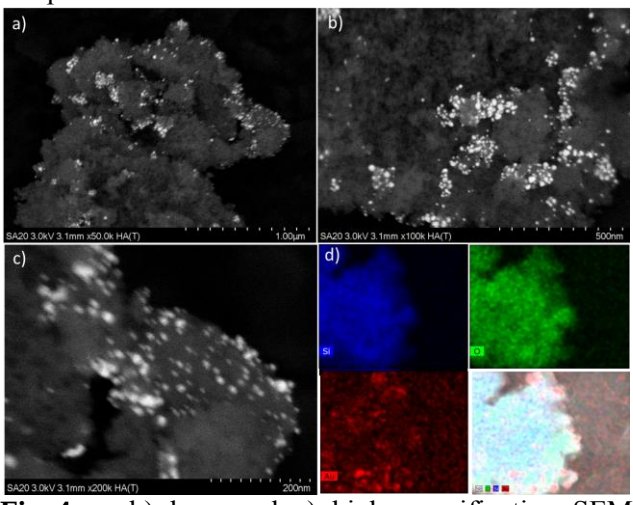

Fig 4. a, b) low, and c) high-magnification SEM images of mesoporous Au/SiO_2 nanocomposite. d) EDS-elemental mapping of Au/SiO_2 nanocomposite showing elements of Si (blue), O (green), Au (red), and overlay of Si, O, and Au elements.

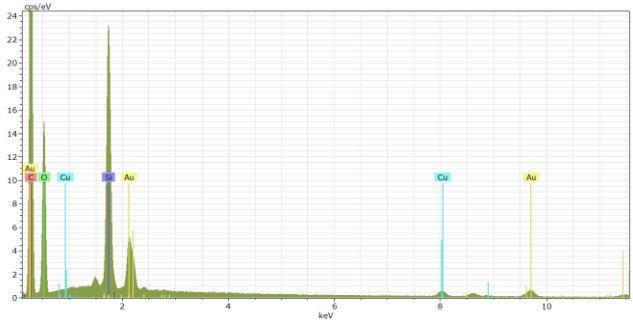

Fig. 5 EDS spectrum of Au/SiO_2 nanocomposite (SA2)

3.4 Optical properties

Fig. 6 shows the absorption spectra of SiO_2 and Au/SiO_2 powder samples. For SiO_2, no surface plasmon resonance (SPR) peak is found, while for Au/SiO_2 samples, the plasmon band is observed at 518 nm and 521 nm for SA1 and SA2, respectively. By increasing the gold precursor concentration, the SPR band broadens and is shifted towards longer wavelength, suggesting the formation of larger gold nanoparticles with high polydispersity.

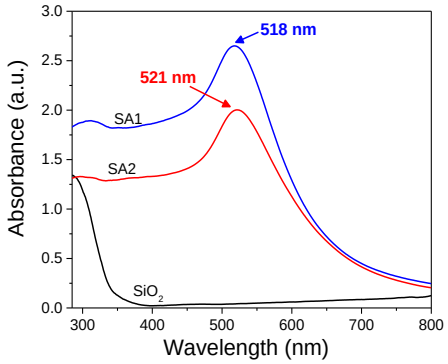

Fig. 6. Diffuse reflectance UV-vis absorption spectra of SiO_2 and Au/SiO_2 nanoparticles.

3.5 Catalytic activity of Au/SiO_2

Fig. 7a shows the UV-vis absorption spectra of 4-nitrophenol solution before and after adding $NaBH_4$. The peak at 317 nm shifts to 400 nm, indicating the formation of nitrophenolate ions. Fig. 7b shows the evolution of UV-visible absorption spectra of 4-nitrophenolate ion immediately after adding $NaBH_4$ and after 24 h addition of borohydride in absence of catalyst. There is no significant change in the intensity of 400 nm peak, confirming that reduction process did not proceed by $NaBH_4$ alone.

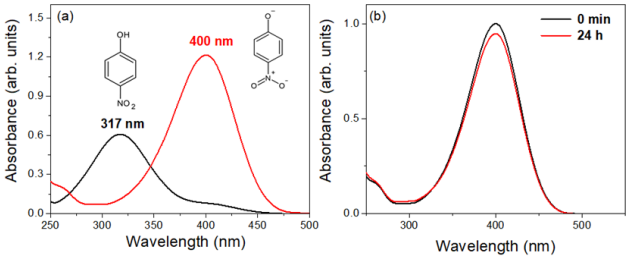

Fig. 7. (a) UV-vis absorbance spectra of the aqueous solution of 4-NP before and after addition of $NaBH_4$ and (b) UV-vis spectra of 4-NP after adding $NaBH_4$ at 0 min and after 24 h.

Fig. 8 displays the evolution of UV-vis absorption spectra of 4-NP using SiO_2 and Au/SiO_2 as catalysts. When SiO_2 was used, there was no change in absorbance at 400 nm within 30 min (Fig. 8a). However, when Au/SiO_2 was added, the absorbance at 400 nm peak decreased gradually with the simultaneous increase in the absorbance of 300 nm peak, suggesting the reduction of 4-NP to 4-aminophenol (4-AP). The solution was almost colorless within 16 min and 18 min using SA1 and SA2 catalysts, respectively.

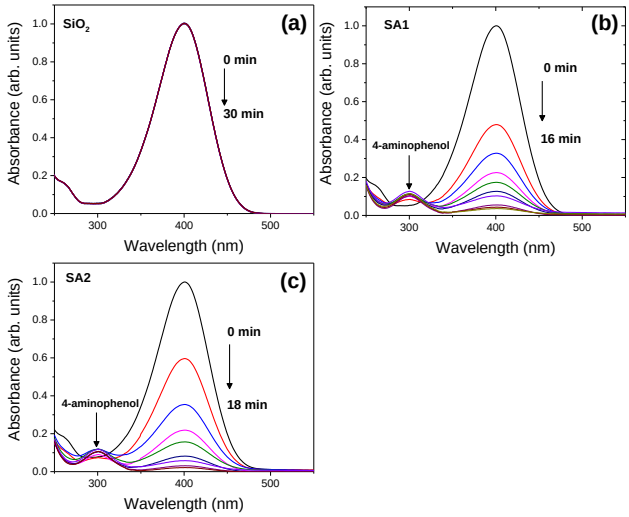

Fig. 8. Time-dependent UV-vis absorption spectra of 4-nitrophenol after adding SiO_2 (a) and Au/SiO_2 catalysts: SA1 (b) and SA2 (c).

Fig 9 shows the dependence of C_t/C_0 versus reaction time at the peak position of 400 nm, where C_t is concentration of 4-NP at time t and C_0 is the initial concentration. It is evident that bare SiO_2 does not have any catalytic activity, whereas Au/SiO_2 manifested high catalytic efficiency towards 4-NP reduction, being SA1 has superior catalytic performance than SA2. Because the $NaBH_4$ concentration is much higher compared to catalyst amount, the reaction rate is assumed to be independent of $NaBH_4$ concentration and a pseudo-first order reaction kinetics can be applied to estimate the reaction rate. Fig. 9b. shows the plot of ln (C_t/C_0) versus reaction time, indicating a linear relationship which is in accordance with first order reaction kinetics. The rate constant, k is estimated as 3.04 x 10^{-1} and 2.17 x 10^{-1} min^{-1} for SA1 and SA2, respectively. The higher catalytic efficiency of SA1 than SA2 can be related to smaller Au NPs in SA1 sample. The observed *k* values are much higher than that reported for other Au/SiO_2 catalyst used in 4-NP reduction [24].

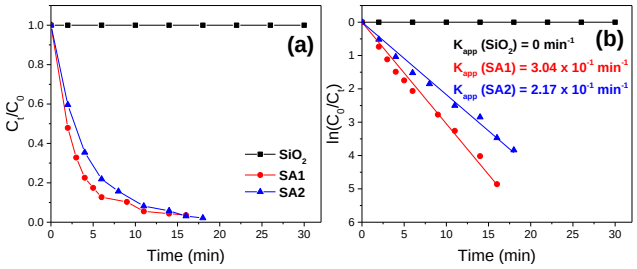

Fig. 9 (a) Decoloration (C_t/C_0) vs time plot and (b) plots of *ln* (C_t/C_0) *vs* reaction time for the reduction of 4-nitrophenol over SiO_2 and Au/SiO_2 catalysts.

4 Conclusion

In summary, gold loaded SiO_2 nanostructure were synthesized by eutectic solvent assisted solvothermal synthesis of mesoporous SiO_2 coupled with borohydride reduction of gold ions and the effect of gold nanoparticles towards the catalytic reduction of 4-nitrophenol was investigated. The high surface area of SiO_2 was helpful to deposit large density of metal nanoparticles on it. By increasing gold precursor, larger size, wide size distribution and higher density of gold nanoparticles are formed on SiO_2 surface in comparison with that obtained using lower $HAuCl_4$ concentration. While SiO_2 nanoparticles did not exhibit any catalytic activity, Au/SiO_2 composite with smaller Au particle size manifested highest catalytic activity towards the reduction of 4-nitrophenol with first-order kinetic rate constant of 0.304 min^{-1}.

References:

[1] H. Qian, L.A. Pretzer, J.C. Velazquez, Z. Zhao, M.S. Wong, *Journal of Chemical Technology & Biotechnology*, Vol. 88, 2013, pp. 735 – 741.

[2] W. Jacak, J. Krasnyj, J. Jacak, W Donderowicz, L Jacak, *Journal of Physics D: Applied Physics*, Vol. 44, 2011, pp. 055301.
[3] M. Holzinger, A. Le Goff, S. Cosnier, *Frontiers in Chemistry*, Vol. 7, 2019, Article 702.
[4] C. Tao, *Letters in Applied Microbiology*, Vol. 67, 2018, pp. 537 – 543.
[5] E.A. Flores-Johnson, J.G. Carrillo, C. Zhai, R.A. Gamboa, Y. Gan, L. Shen, *Scientific Reports*, Vol. 8, 2018, Article number: 9668.
[6] S.B. ManiKanth, K. Kalishwaralal, M. Sriram, S.B.R.K. Pandian, H-S. Youn, S-H. Eom, S. Gurunathan, *Journal of Nanobiotechnology*, Vol. 8, 2010, Article number: 16.
[7] N. Kapil, F. Cardinale, T. Weissenberger, P. Trogadas, T.A. Nijhuis, M.M. Nigra, M.O. Coppens, *Chemical Communication*, Vol. 57, 2021, pp. 10775 – 10778.
[8] S. Wei, X-P. Fu, W-W. Wang, Z. Jin, Q-S Song, C-J. Jia, *The Journal of Physical Chemistry C*, Vol. 122, 2018, pp. 4928 – 4936.
[9] S. Lomate, A. Sultana, T. Fujitani, *Catalysis Science and Technology*, Vol. 7, 2017, pp. 3073 – 3083.
[10] K.M. Saoud, M.S. El-Shall, *Catalysts*, Vol. 10, 2020, pp. 1351 - 1372.
[11] R.K. Sharma, S. Dutta, S. Sharma, R. Zboril, R.S. Varma, M.B. Gawande, *Green Chemistry*, Vol. 18, 2016, pp. 3184 – 3209.
[12] K. Liu, R. Qin, L. Zhou, P. Liu, Q. Zhang, W. Jing, P. Ruan, L. Gu, G. Fu, N. Zheng, *CCS Chemistry*, Vol. 1, 2019, pp. 207 – 214.
[13] M. Marturano, E.F. Aglietti, O. Ferretti, *Materials Chemistry and Physics*, Vol. 47, 1997, pp. 252 – 256.
[14] F. Zhang, P. Yang, K. Matras-Postolek, J. *Nanoscence and Nanotechnology*, Vol. 16, 2016, pp. 5966 – 5974.
[15] I.A. Rahman, V. Padavettan, *Journal of Nanomaterials*, Vol. 2012, 2012, Article number: 8.
[16] T. Tani, N. Watanabe, K. Takatori, *Journal of Nanoparticle Research*, Vol. 5, 2003, pp. 39 – 46.
[17] X. Li, J. Choi, W-S Ahn, K.H. Row, Critical Reviews in Analytical Chemistry, Vol. 48, 2018, pp. 73 – 85.
[18] S.K. Krishnan, M.G-F. Garcia, E. Prokhorov, M. Estevez-González, R. Pérez, R. Esparza, M. Meyyappan, *Journal of Materials Chemistry B*, Vol. 5, 2017, pp. 7072 – 7081.
[19] R.T. Ayinla, J.O. Dennis, H.M. Zaid, Y.K. Sanusi, F. Usman, L.L. Adebayo, *Journal of Cleaner Production*, Vol. 229, 2019, pp. 1427 – 1442.
[20] B. Thongma, S Chiarakorn, *Earth and Environmental Science*, Vol. 373, 2019, Article number: 012026.
[21] S. Wen, L. Liu, L. Zhang, Q. Chen, L. Zhang, H. Fong, *Materials Letters*, Vol. 64, 2010, pp. 1517 – 1520.
[22] J. Cui, H. Sun, Z. Luo, J. Sun, Z. Wen, *Materials Letters*, Vol. 156, 2015, pp. 42 – 45.
[23] A. Arshad, J. Iqbal, Q. Mansoor, I. Ahmed, Journal of Applied Physics, Vol. 121, 2017, Article number: 244901.
[24] J. Hao, B. Liu, S. Maenosono, J. Yang, Scientific Reports, Vol. 12, 2022, pp. 7615 – 7626.

Acknowledgement: The authors are thankful for the financial support received through VIEP-BUAP 2021 project (Grant#100468355). Andrés Guzmán Cruz (CVU # 862151) is thankful to CONACYT for extending doctoral scholarship in Materials Science.